Journal of The Electrochemical Society, **159** (6) D362-D366 (2012)
0013-4651/2012/159(6)/D362/5/$28.00 © The Electrochemical Society

The Formation and the Plane Indices of Etched Facets of Wet Etching Patterned Sapphire Substrate

Yu-Chung Chen,[a] Feng-Ching Hsiao,[a] Bo-Wen Lin,[a] Bau-Ming Wang,[a] YewChung Sermon Wu,[a,*,z] and Wen-Ching Hsu[b]

[a]*Department of Materials Science and Engineering, National Chiao Tung University, Hsinchu 300, Taiwan*
[b]*Sino-American Silicon Products Inc., Hsinchu, Taiwan*

A two-step chemical wet etching processes were used to investigated the formation and the plane indexes of exposed etched facets of wet etching patterned sapphire substrate (PSS). It was found when SiO_2 mask still remained on the top *c*-plane, the structure of PSS comprised of a hexagonal pyramid covered with six facets $\{3\bar{4}17\}$ with a flat top *c*-plane. When SiO_2 mask were etched away, beside six facets on the bottom, there were 3 extra facets $\{1\bar{1}05\}$ exposed on the top.
© 2012 The Electrochemical Society. [DOI: 10.1149/2.095206jes] All rights reserved.

Manuscript submitted December 22, 2011; revised manuscript received February 28, 2012. Published April 10, 2012.

Light-emitting diodes (LEDs) are expected to play an important role in next-generation light source due to their advantages of high efficiency, long life, small size, environmental protection, various colors and wide applications. In particular, high-brightness GaN-based LEDs have attracted considerable attention for white light solid-state lighting. Many techniques have been developed for improving GaN-based LEDs internal quantum efficiency (IQE) and light extraction efficiency (LEE), such as epitaxial lateral overgrowth, surface roughing, metal mirror reflect layer and patterned sapphire substrate (PSS).[1–9] Currently, the PSS technique has attracted much attention for its high production yield. Besides, using the PSS technique can improve both IQE and LEE.[10–15]

Two kinds of etching methods have been used to fabricate PSS :(1) dry etching and (2) wet etching. In dry etching, the ion bombardment caused damages on PSS surface and resulted in an increased of threading dislocations propagating through the GaN epitaxial layers.[16,17] On the other hand, wet etching did not have this ion damage problem. Besides, wet etching method can also reduce the fabrication cost of PSS and simplify the process.[18–20] In wet etching, the sapphire substrate covered with SiO_2 hard mask is usually etched by a mixed solution of hot H_2SO_4 and H_3PO_4.

After etching, several etched facets were exposed. These facets have been identified differently as *n*-like plane,[21,22] *r*-like plane,[13,23] and mixture of *m*-, *r*- and *a*-like plane.[24] It has been found beside normal wurtzite GaN, zincblende GaN has been found on these planes of PSS.[20] Therefore, in this study, the formation and plane indexes of these exposed etched facets were investigated by a two-step etching process.

Experimental

PSSs with periodic dot array patterns (1-μm width and 2-μm spacing) were prepared by standard photolithography. A 400-nm-thick SiO_2 film served as the wet-etching hard mask and was deposited on the sapphire surface by plasma-enhanced chemical vapor deposition (PECVD). The substrate with SiO_2 mask was immersed in a H_3PO_4-based etchant at 270°C for various times (11, 12, 14 and 16 min). They were denoted as 11, 12, 14 and 16PSS. The surface morphology of the PSS was observed and measured by scanning electron microscope (SEM) and focused ion beam (FIB).

Result and Discussion

Figure 1 shows the SEM images of 12PSS. As shown in Fig. 1a, the structure of 12PSS comprises of a hexagonal pyramid covered with six facets with a flat top *c*-plane. After 12PSS was dipped into buffered oxide etchant (BOE) to remove the SiO_2, top *c*-planes were clearly shown on Figs. 1b and 1c. These six planes were designated "6-bottom" (6B) planes. The cross section image of 6B planes is shown on Fig. 1d. The slanted angle between the intersections of 6B planes and *c*-plane was around 57.3°.

The SEM images of 14PSS were shown in Fig. 2a and 2b. No top *c*-plane was found on these structures. In addition to 6B facets, three facets were found on the top of 6B facets. These three facets were designated "3-top" (3T) planes. As shown in Fig. 2c, the slanted angle between the 3T planes and *c*-plane was around 31.9° while the angle of the 6B planes was still around 57.3°.

As the etching time increased, the areas of 3T facets increased and at the same time those of 6B decreased. When etching time reached 16 min, only few 6B facets were left as shown in Fig. 3a and 3b. As shown in Fig. 3c, the angle of the 3T planes was around 32.1°.

The increase of 3T areas (decrease of 6B areas) might have resulted from the removing of SiO_2 hard mask during the etching process since H_3PO_4 can etch SiO_2 and sapphire simultaneously.[23,25] A two-step etching process was used to test this assumption. In the first step, sample was etching for 11 min. As shown in Fig. 4a and 4b, 11PSS is composed of pyramid with a top *c*-plane. The height of 11PSS pyramid was 1.55 μm (not include SiO_2 thickness), which was less than that of 12PSS (1.77 μm). This is because the etching depth (pyramid height) was increased with the etching time. The top *c*-plane area of 11PSS was the same as that of 12PSS since SiO_2 hard mask still remained on the top *c*-plane.

Before second etching step, 11PSS was dipped into BOE to remove the SiO_2 mask. Sample was then etched in same solution for another 3 min. It was designated as "3+11PSS". As shown in Fig. 4c to 4e, compared with 14PSS, even though the total etching time was the same, the height of 3+11PSS was lower than that of 14PSS. This is because top *c*-plane was also etched by H_3PO_4–based solution during the second etching step. On the other hand, the 3T area of 3+11PSS was larger than that of 14PSS. This is because in 3+11PSS, oxide was removed after 11 min, while in 14PSS, oxide was not removed until around 12.5 min. In other words, the increase of 3T areas (decrease of 6B areas) was due to the removing of SiO_2 hard mask during the etching process.

The sapphire etching mechanism was schematically illustrated in Fig. 5. When the SiO_2 mask still remained on the top *c-plane,* the etching rate of 6B planes was very slow compared with the vertical etching rate of bottom *c-plane.* As a result the size (height) of pyramid increased with the etching time (Fig. 5a). When SiO_2 mask was gone (etched away), top *c-plane* was also etched by H_3PO_4–based solution. At the same time, 3T facets appeared. As a result, as the etching time increased, the size (height) of pyramid decreased and the 3T areas increased (Fig. 5b). Besides, it is worthy to note that the slanted angles of 6B and 3T planes did not change with the etching time as shown in Fig. 1d, Fig. 2c and Fig. 3c.

*Electrochemical Society Active Member.
zE-mail: SermonWu@StanfordAlumni.org

Downloaded on 2014-04-28 to IP 140.113.38.11 address. Redistribution subject to ECS terms of use (see ecsdl.org/site/terms_use) unless CC License in place (see abstract).

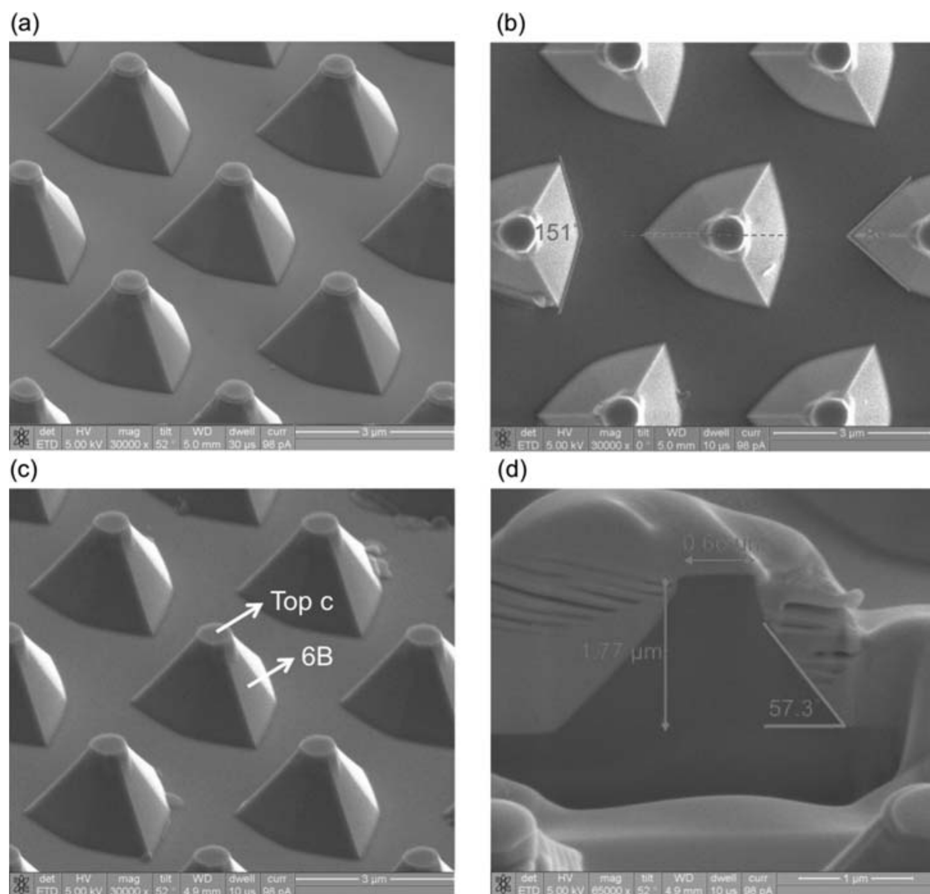

Figure 1. SEM images of 12PSS. (a) is the side-view image before removing of SiO_2 layer (viewed from 52° to sample normal). (b) and (c) are the top-view and side-view images after removing of SiO_2. (d) is the cross-section image from (b) indicated by dash lines along $(1\bar{2}10)$ after removing of SiO_2.

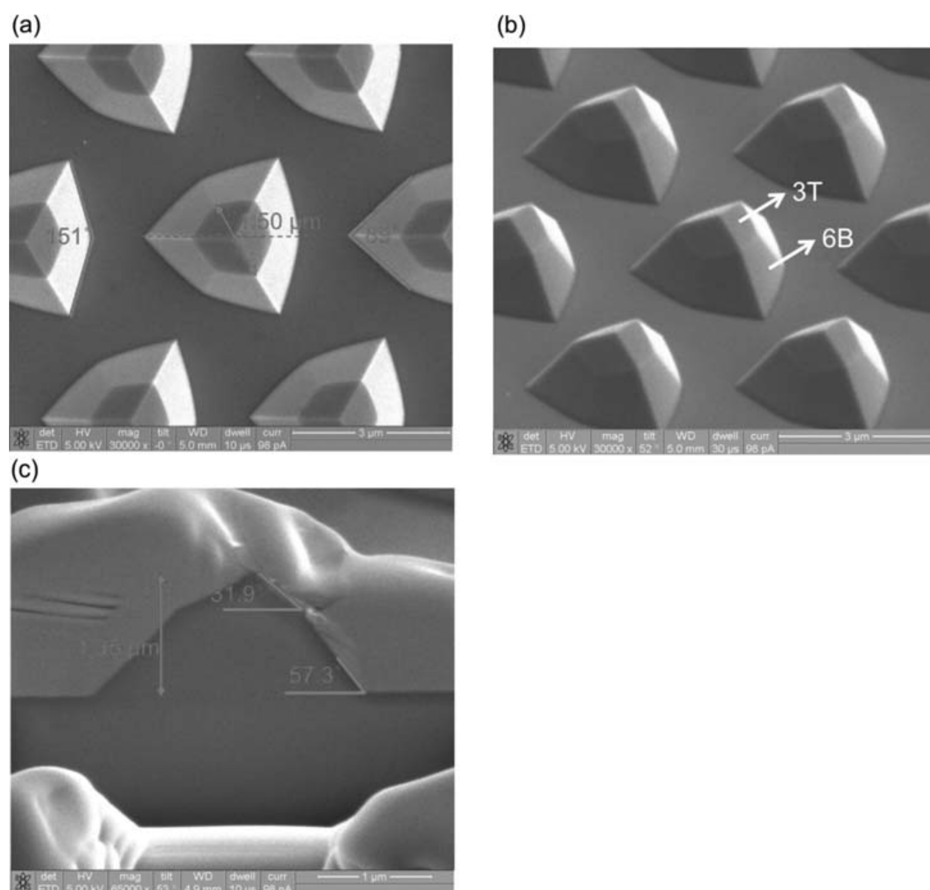

Figure 2. SEM images of 14PSS. (a) is the top-view image. (b) is the side-view image. (c) is the cross-section image.

Downloaded on 2014-04-28 to IP 140.113.38.11 address. Redistribution subject to ECS terms of use (see ecsdl.org/site/terms_use) unless CC License in place (see abstract).

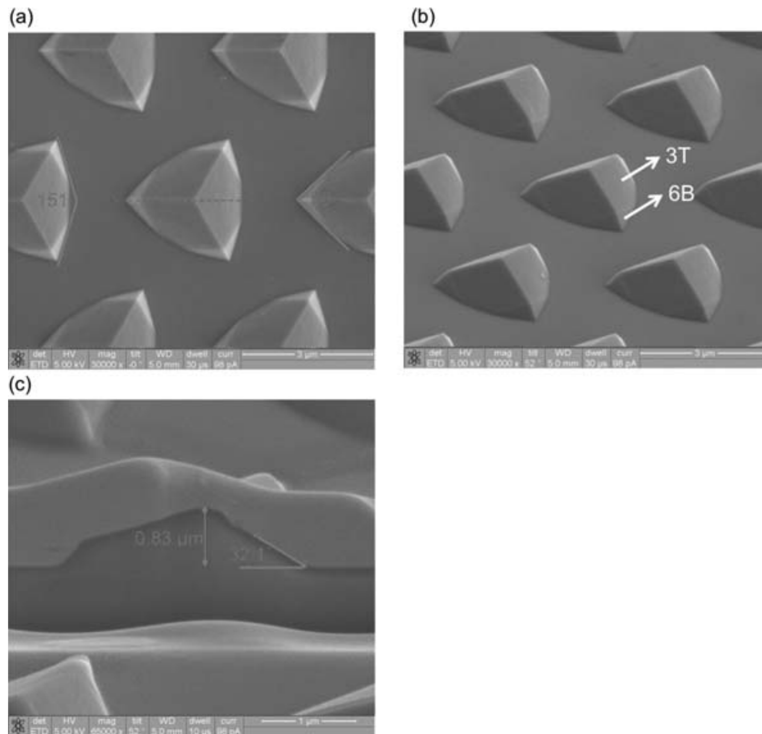

Figure 3. SEM images of 16PSS. (a) is the top-view image. (b) is the side-view image. (c) is the cross-section image.

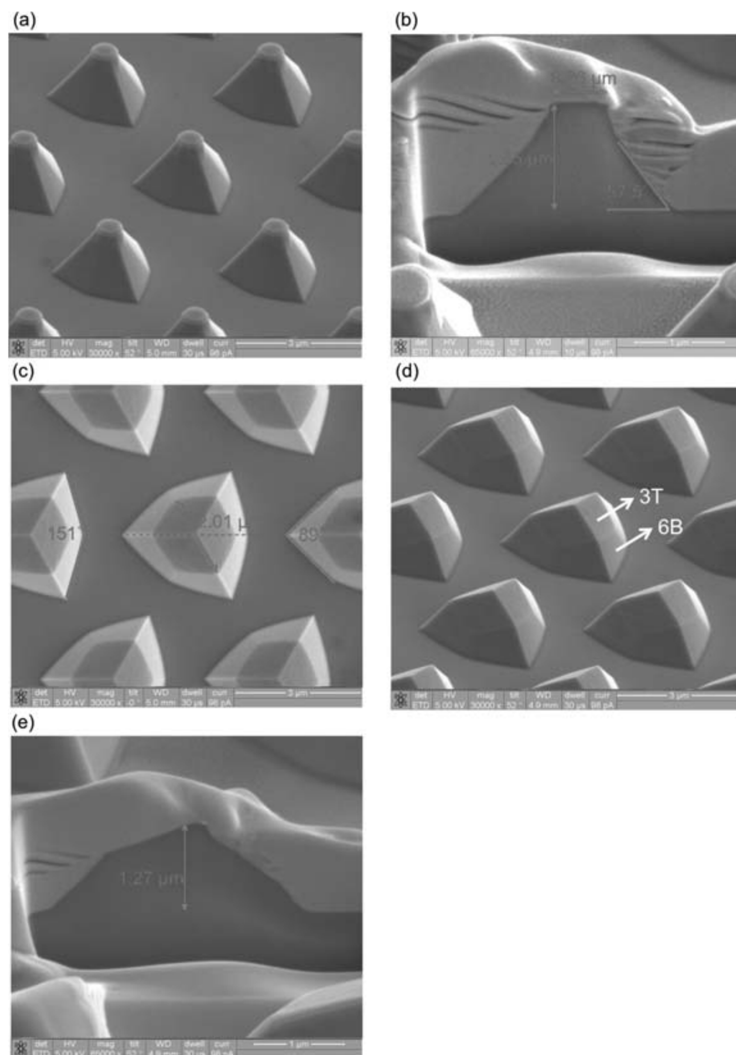

Figure 4. SEM images of 11PSS[(a) and (b)] and 3+11PSS[(c), (d) and (e)]. (a) is the side-view, and (b) is the cross-section images of 11PSS. (c) is the top-view, (d) is the side-view, and (d) is the cross-section images of 3+11PSS.

Downloaded on 2014-04-28 to IP 140.113.38.11 address. Redistribution subject to ECS terms of use (see ecsdl.org/site/terms_use) unless CC License in place (see abstract).

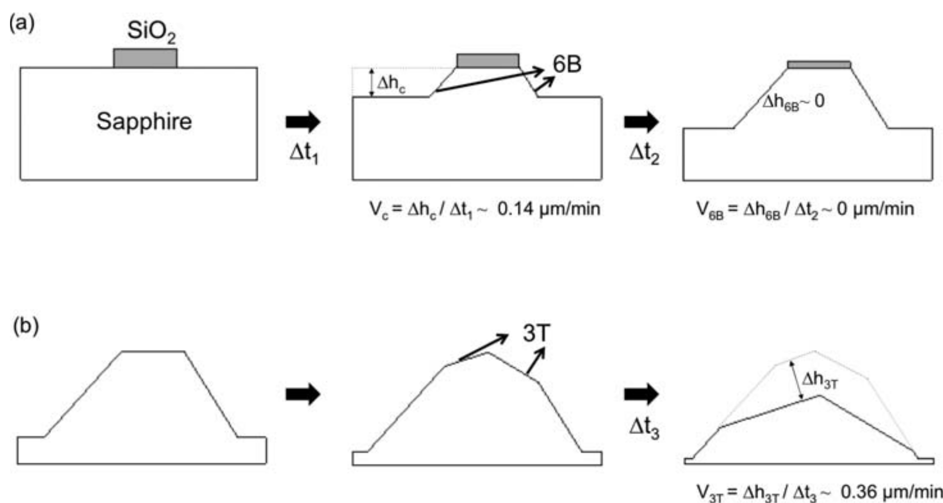

Figure 5. Schematic illustrations of etching process when (a) the SiO_2 still on the top c-plane, and (b) the SiO_2 was totally etched away.

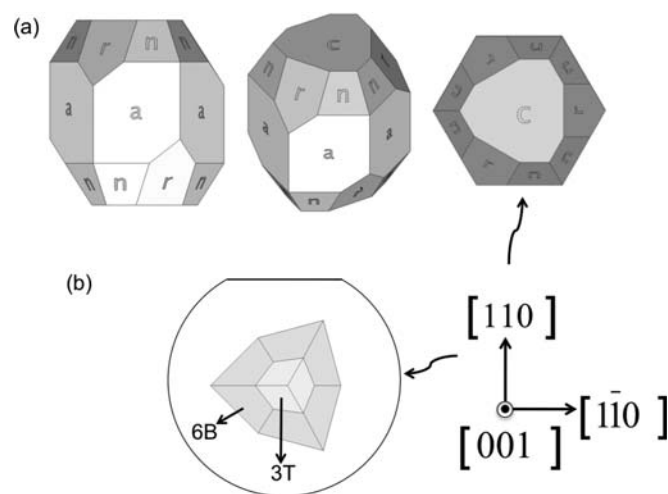

Figure 6. (a) is the crystallographic diagrams of sapphire. (b) is the relative orientations and projections of 6B and 3T structure on (0001) plane.

There are 3 different planes appeared in the wet etching process, *c*, 6B and 3T planes. The etching rate was calculated by the cross-sectional SEM images. As illustrated in Fig. 5a, the etching rate of *c*-plane (V_c) was ~0.14 μm/min. The etching rate of 6B planes (V_{6B}) was ~0 μm/min. This is because when SiO_2 mask remained on the top *c*-plane, there was almost no change of top *c*-plane diameter. The etching rate of 3T planes (V_{3T}) was ~0.36 μm/min as illustrated in Fig. 5b.

To investigate 6B and 3T, the crystallographic planes of sapphire from different view angles are illustrated in Fig. 6a. The related observed projections of 6B and 3T planes on sapphire wafer are shown in Fig. 6b. Compared Figs. 2 with Fig. 6, 3T planes could belong to the *r*–like planes. However, 6B planes are neither *n*–like nor *r*–like plane.

The detailed analysis of the hexagonal pyramid is illustrated in Fig. 7. The intercepts of the 6B plane on the a_1, a_3 and c axes are about 3.000, 8.196 and 3.514 units. The intercepts of the 3T plane on the a_1, a_2 and c axes are about 4.914, −4.914 and 2.558 units, respectively.

In hexagonal crystals, the Miller-Bravais indexes of a plane are denoted by (*hkil*). These indexes are the reciprocals of intercepts on the a_1, a_2, a_3 and c, respectively. The additional condition which their values must satisfy is $h + k = -i$. Then, take the reciprocals of these numbers in Fig. 7, and multiplied with sapphire's unit length ($a = 4.759$ Å and $c = 12.991$ Å).[26] The calculated Miller-Bravais indexes of 6B and 3T planes are $\{3\bar{4}17\}$ and $\{1\bar{1}05\}$, respectively.

These 6B and 3T plane indexes were confirmed by calculating the angles among 6B, 3T and *c*-planes. The angle, φ, between two crystal planes $(h_1k_1i_1l_1)$ and $(h_2k_2i_2l_2)$ is given by[26]

$$\phi = \cos^{-1}\left[\frac{h_1h_2 - (h_1k_2 + h_2k_1)/2 + k_1k_2 + \frac{3a^2}{4c^2}l_1l_2}{\left(h_1^2 - h_1k_1 + k_1^2 + \frac{3a^2}{4c^2}l_1^2\right)^{1/2}\left(h_2^2 - h_2k_2 + k_2^2 + \frac{3a^2}{4c^2}l_2^2\right)^{1/2}}\right]$$

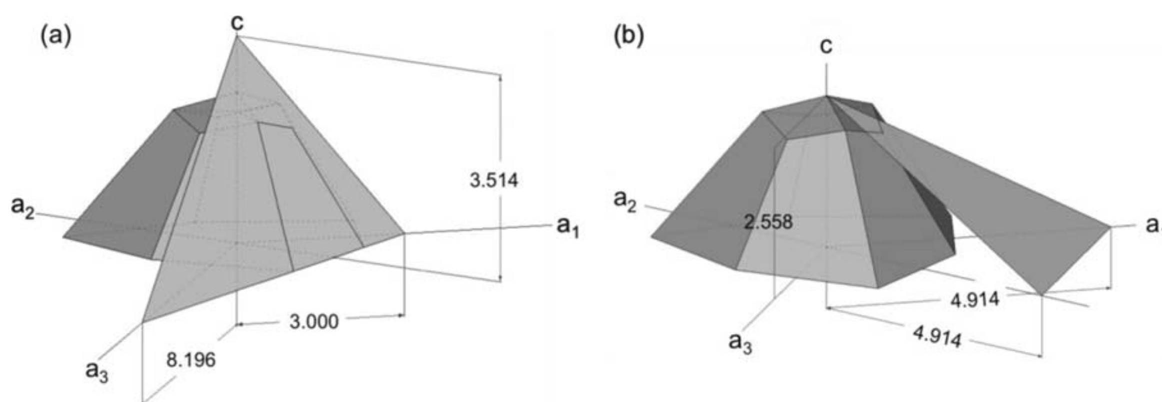

Figure 7. The intercepts of (a) 6B and (b)3T plane on the axes.

Downloaded on 2014-04-28 to IP 140.113.38.11 address. Redistribution subject to ECS terms of use (see ecsdl.org/site/terms_use) unless CC License in place (see abstract).

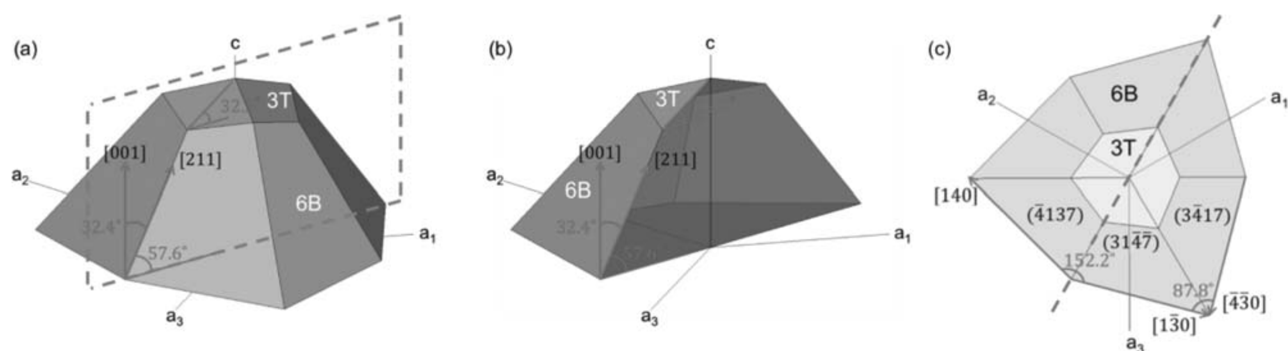

Figure 8. Schematic illustrations of hexagonal pyramid. (a) is the side-view illustration. (b) is the cross-section illustration from (a) and (c) indicated by dash lines. (c) is the projection of hexagonal pyramid on (0001) plane.

The calculated angle between 3T planes $\{1\bar{1}05\}$ and *c*-plane (0001) was 32.2° as shown in Figs. 8a and 8b. This angle was almost the same as those angles observed in Figs. 2c and 3c.

Before confirmed the angle between 6B planes and *c*-plane, we needed calculated the intersection directions of 6B planes. As illustrated in Figs. 8a and 8b, one of these directions, [211], can be calculated by cross product of normal direction of $(\bar{4}137)$ and $(31\bar{4}\bar{7})$. The angle, θ, between two directions $[u_1v_1w_1]$ and $[u_2v_2w_2]$ is given by[26]

$$\theta = \cos^{-1}\left[\frac{u_1u_2 - (u_1v_2 + u_2v_1)/2 + v_1v_2 + \frac{c^2}{a^2}w_1w_2}{\left(u_1^2 - u_1v_1 + v_1^2 + \frac{c^2}{a^2}w_1^2\right)^{1/2}\left(u_2^2 - u_2v_2 + v_2^2 + \frac{c^2}{a^2}w_2^2\right)^{1/2}}\right]$$

The calculated angle between [211] and [001] (normal direction of c-plane) was 32.4°. In other words, the angle of cross-section was 57.6° as illustrated in Figs. 8a and 8b. This angle was almost the same as those angles observed in Figs. 1d, 2c, and 4b.

The projection of pyramid on (0001) plane was illustrated in Fig. 8c. The intersection directions of 6B planes and c-plane were calculated by cross product of normal directions of these planes.[26] Some of these intersection directions ([140], $[1\bar{3}0]$ and $[\bar{4}\bar{3}0]$) were illustrated in Fig. 8c. The calculated angle between [140] and $[1\bar{3}0]$ was 152.2°, while that between $[1\bar{3}0]$ and $[\bar{4}\bar{3}0]$) was 87.8°. These angles were almost the same as those angles observed in Figs. 1b, 2a, 3a, and 4c.

Conclusions

Wet etching PSS substrates have been used to improve both IQE and LEE of GaN-based LEDs. In wet etching process, several etched facets were exposed on PSSs. In this study, a two-step wet etching processes were used to investigated the formation mechanism and the plane indexes of these exposed facets. It was found that, when SiO_2 mask remained on the top *c*-plane, PSS has a three-dimensional structure, which is composed of a hexagonal pyramid covered with six 6B facets. The plain indexes of 6B were $\{3\bar{4}17\}$. When SiO_2 mask were etched away, three 3T facets were found on the top of 6B facets. The plain indexes of 3T were $\{1\bar{1}05\}$.

Acknowledgments

This project was funded by Sino American Silicon Products Incorporation and the National Science Council of the Republic of China under grant No. 98-2221-E009-041-MY3. Technical supports from the National Nano Device Laboratory, Center for Nano Science and Technology, Nano Facility Center and Semiconductor Laser Technology Laboratory of the National Chiao Tung University are also acknowledged. The authors thank H. C. Kuo for valuable discussions.

References

1. A. Sakai, H. Sunakawa, and A. Usui, *Appl. Phys. Lett.*, **71**, 2259 (1997).
2. K. Linthicum, T. Gehrke, D. Thomson, E. Carlson, P. Rajagopal, T. Smith, D. Batchelor, and R. Davis, *Appl. Phys. Lett.*, **75**, 196 (1999).
3. M. Boroditsky and E. Yablonovitch, *Proc. SPIE*, **3002**, 119 (1997).
4. W. C. Peng and Y. S. Wu, *Appl. Phys. Lett.*, **88**, 181117 (2006).
5. C. E. Lee, Y. J. Lee, H. C. Kuo, M. R. Tsai, B. S. Cheng, T. C. Lu, S. C. Wang, and C. T. Kuo, *IEEE Photon. Technol. Lett.*, **19**, 1200 (2007).
6. H. W. Huang, C. H. Lin, C. C. Yu, B. D. Lee, C. H. Chiu, C. F. Lai, H. C. Kuo, K. M. Leung, T. C. Lu, and S. C. Wang, *Nanotechnology*, **19**, 185301 (2008).
7. Y. S. Wu, C. Liao, and W. C. Peng, *Electrochem. Solid-State Lett.*, **10**, J126 (2007).
8. D. S. Han, J. Y. Kim, S. I. Na, S. H. Kim, K. D. Lee, B. Kim, and S. J. Park, *IEEE Photon. Technol. Lett.*, **18**, 1406 (2006).
9. S. J. Chang, C. S. Chang, Y. K. Su, R. W. Chuang, W. C. Lai, C. H. Kuo, Y. P. Hsu, Y. C. Lin, S. C. Shei, H. M. Lo, J. C. Ke, and J. K. Sheu, *IEEE Photon. Technol. Lett.*, **16**, 1002 (2004).
10. D. S. Wuu, W. K. Wang, W. C. Shih, R. H. Horng, C. E. Lee, W. Y. Lin, and J. S. Fang, *IEEE Photon. Technol. Lett.*, **17**, 288 (2005).
11. Z. H. Feng and K. M. Lau, *IEEE Photon. Technol. Lett.*, **17**, 1812 (2005).
12. Y. J. Lee, T. C. Hsu, H. C. Kuo, S. C. Wang, Y. L. Yang, S. N. Yen, Y. T. Chu, Y. J. Shen, M. H. Hsieh, M. J. Jou, and B. J. Lee, *Mater. Sci. Eng. B*, **122**, 184 (2005).
13. Y. J. Lee, J. M. Hwang, T. C. Hsu, M. H. Hsieh, M. J. Jou, B. J. Lee, T. C. Lu, H. C. Kuo, and S. C. Wang, *IEEE Photon. Technol. Lett.*, **18**, 1152 (2006).
14. K. Tadatomo, H. Okagawa, Y. Ohuchi, T. Tsunekawa, Y. Imada, M. Kato, and T. Taguchi, *J. Jpn. Appl. Phys.*, **40**, L583 (2001).
15. M. Yamada, T. Mitani, Y. Narukawa, S. Shioji, I. Niki, S. Sonobe, K. Deguchi, M. Sano, and T. Mukai, *J. Jpn. Appl. Phys.*, **41**, L1431 (2002).
16. M. Kappelt and D. Bimberg, *J. Electrochem. Soc.*, **143**, 3271 (1996).
17. J. Wang, L. W. Guo, H. Q. Jia, Z. G. Xing, Y. Wang, H. Chen, and J. M. Zhou, *J. Jpn. Appl. Phys.*, **44**, L982 (2005).
18. D. S. Wuu, W. K. Wang, K. S. Wen, S. C. Huang, S. H. Lin, S. Y. Huang, C. F. Lin, and R. H. Horng, *Appl. Phys. Lett.*, **89**, 161105 (2006).
19. Y. J. Lee, H. C. Kuo, T. C. Lu, B. J. Su, and S. C. Wang, *J. Electrochem. Soc.*, **153**, G1106 (2006).
20. J. H. Cheng, Y. S. Wu, W. C. Liao, and B. W. Lin, *Appl. Phys. Lett.*, **96**, 051109 (2010).
21. R. M. Lin, Y. C. Lu, S. F. Yu, Y. S. Wu, C. H. Chiang, W. C. Hsu, and S. J. Chang, *J. Electrochem. Soc.*, **156**, H874 (2009).
22. H. Gao, F. Yan, Y. Zhang, J. Li, Y. Zeng, and G. Wang, *J. Appl. Phys.*, **103**, 014314 (2008).
23. D. S. Wuu, W. K. Wang, K. S. Wen, S. C. Huang, S. H. Lin, R. H. Horng, Y. S. Yu, and M. H. Pan, *J. Electrochem. Soc.*, **153**, G765 (2006).
24. S. H. Huang, R. H. Horng, K. S. Wen, Y. F. Lin, K. W. Yen, and D. S. Wuu, *IEEE Photon. Technol. Lett.*, **18**, 2623 (2006).
25. W. V. Gelder and V. E. Hauser, *J. Electrochem. Soc.*, **114**, 869 (1967).
26. W. E. Lee and K. P. D. Lagerlof, *J. Electron Microsc. Tech.*, **2**, 247 (1985).

Downloaded on 2014-04-28 to IP 140.113.38.11 address. Redistribution subject to ECS terms of use (see ecsdl.org/site/terms_use) unless CC License in place (see abstract).